Journal of Polymers and the Environment
https://doi.org/10.1007/s10924-024-03274-w

ORIGINAL PAPER

Processing and Evaluation of Bio-Based Paramylon Ester/Poly(butylene succinate) Blends for Industrial Applications

Manikandan Ilangovan[1] · **Taizo Kabe**[1] · **Tadahisa Iwata**[1]

Accepted: 3 April 2024

Abstract

Poly(butylene succinate) (PBS) was melt-blended with paramylon based mixed ester, paramylon propionate hexanoate (PaPrHe) and characterized for its morphology, thermal and mechanical properties. The PBS/PaPrHe blends were found to be immiscible throughout the loading range of PaPrHe (10–90 wt%), with individual glass transition peaks. Due to the immiscibility, there was phase separation observed in the bulk, evident by sea-island morphology. However, further observation of the micro-structure revealed that, in low PaPrHe loading (10–30 wt%), there was a micron to sub-micron order distribution of PBS particles and partially miscible PBS/PaPrHe phase. On increasing the PaPrHe to 50 wt% and beyond, the sub-micron scale domains fused to form a co-continuous morphology. As a result, the impact strength of PBS increased from 6.6 to 16.4 kJ/m^2 in the 50/50 blend. Under tensile loading, the strength at break and elongation decreased after the introduction of less-flexible PaPrHe particles in the blend. This could be countered by uniaxially stretching the blended films with 10–30 wt% PaPrHe, after which the tensile strength increased by up to 380% (from 33–52 MPa to 165–200 MPa) compared to the unstretched films, attributable to the increased degree of orientation of the molecular chains. In terms of thermal processability, all the blend ratios had high thermal degradation temperature (>350 °C), higher than the melt-flow temperature (124–133 °C) providing a wide processing window. Overall, PBS/PaPrHe blend is a novel bio-based blend with properties suitable for packaging, mulching, and related applications.

Keywords Poly(butylene succinate) · Paramylon ester · Toughness · Enzymatic etching · Blends

Introduction

Rising global awareness of the environmental issues of plastics and its associated carbon emissions is fueling the transition to sustainable plastics derived from renewable resources [1, 2]. Bioplastics, which is an umbrella term for both bio-based and biodegradable plastics, are considered to be an effective alternative to the conventional fossil-fuel based plastics. Commercial examples include poly(lactic acid) (PLA), thermo-plastic starch, polysaccharide esters such as cellulose triacetate (CTA), polyhydroxyalkanoates (PHAs), polycaprolactone (PCL), poly(butylene succinate) (PBS), poly(butylene succinate-*co*-adipate (PBSA), poly(butylene adipate-*co*-terephthalate) (PBAT) and so on. With the advancements in production technology, growing government attention, and ever fluctuating petroleum market, bioplastics are becoming competitive even in terms of cost as well [3].

PBS is a widely used biodegradable aliphatic polyester with physical properties comparable to several commercial plastics. PBS is synthesized through the polycondensation of succinic acid and 1,4 butanediol [4]. Currently, most of the production of succinic acid is dependent on crude oil making PBS a partially bio-based polymer, nevertheless, there have been successful reports on the synthesis of completely bio-based PBS, making it an important polymer for the future [4, 5]. Its high ductility, and high heat deflection temperature enables it to be used in packaging and mulching applications [3]. However, the impact strength of PBS is relatively low compared to high density polyethylene (HDPE), PBAT and other commercial plastics and bioplastics, due to which the scalability and scope of applications is hampered. To improve the mechanical properties, there are

✉ Tadahisa Iwata
atiwata@g.ecc.u-tokyo.ac.jp

[1] Science of Polymeric Materials, Department of Biomaterial Sciences, Graduate School of Agricultural and Life Sciences, The University of Tokyo, 1-1-1 Yayoi, Bunkyo-ku, Tokyo 113-8657, Japan

Published online: 02 May 2024

several techniques available, but the most resource-effective way is through blending. Polymer blending is a scalable and industrially sought after process to obtain properties that the polymer initially does not provide [6–8]. Blending is also cheaper as it does not require developing or synthesizing new materials. Specific improvement in properties could also be obtained by the inclusion of additives such as compatibilizing and cross-linking agents.

Paramylon is a storage polysaccharide with β-1,3 glycosidic linkage, photosynthesized by *Euglena gracilis* [9]. Because of its acidophilic and heterotrophic nature, *E. gracilis* can photosynthesize paramylon in an acidic, high CO_2 concentration environment, making paramylon a potential carbon neutral biomass of the future [10, 11]. Currently, there are several attempts to mass culture paramylon for various applications [12]. Multiple past reports show that by esterifying the hydroxyl groups of paramylon, bioplastics with varying physical properties could be obtained [9]. Paramylon homoesters with different alkyl chains have also been thoroughly characterized for its molecular structures and physical properties [9]. In a parallel approach, instead of homoesters, paramylon mixed esters with short chain and long chain acyl groups are found to have a good balance between mechanical properties and thermal processability [13, 14]. Paramylon propionate hexanoate (PaPrHe) is a prime example of such mixed esters derivatized from paramylon, with good mechanical properties (tensile strength: 28 MPa), and relatively low processing temperature (140–150 °C) that can be formed into films or injection molded compounds without the need for any additives or organic solvent [15].

Several authors have attempted blending PBS with polysaccharide esters to improve the mechanical properties of PBS. Zhao et al., studied the effects of blending PLA with PBS in an attempt to obtain polymer blend with improved toughness [16]. Results show that PBS/PLA blends had improved thermal and rheological properties with good compatibility when the PBS content ranged between 10 and 20 wt%. In terms of mechanical properties, the highest toughness was also attained when the PBS content was 20 wt%. With further addition of PBS, the compatibility declined leading to inferior mechanical properties [16]. They countered this decline by adding an epoxy-functionalized methyl methacrylate-*co*-glycidyl methacrylate copolymer (PMMA-GMA), as the reactive compatibilizer [17]. After compatibilizing, the micromorphology of 50/50 ratio of PBS/PLA changed significantly affecting the dispersion of PBS in PLA phase. As a direct result of this, the mechanical properties also improved with increasing compatibilizer content. It was seen that the highest toughness (~33 kJ/m^2) was obtained when the compatibilizer loading was kept at 7 wt% [17]. In PBS blends with polysaccharide ester components, adding 15 wt% CTA was shown to improve the tensile modulus of PBS however the elongation at break was reduced drastically [18]. In other reports, addition of cellulose acetate butyrate, a mixed ester of cellulose, acted as a bio-plasticizer in the blend leading to improved mechanical properties [19, 20]. In our previous work, we also reported that blending PBS with paramylon hexanoate (PaHe) led to an improvement in the elongation at break of PBS without any loss in tensile strength. This was attributed to the formation of favorable morphologies in the binary blend system without the use of any compatibilizers or cross-linking agents. Blending PaHe also increased the hydrophobicity of the system making PBS more attractive to the packaging industry [21]. Further, after uniaxial drawing of PBS/PaHe blends, films with significantly improved mechanical properties were obtained.

Typically, uniaxial and biaxial stretching are common industrial techniques to improve the mechanical properties of polymers, including PBS. Vega-Baudrit and co-workers studied the effects of drawing on the properties of PBS [22]. Their work show that the strength at break improved from ~20 MPa in the unstretched PBS to over 250 MPa for a draw ratio (DR) of 4. Further analysis revealed that this improvement was attributable to the increased crystallinity as a result of molecular reorientation in the matrix along the stretching axis [22]. This effect was confirmed in melt-drawing of PBS as well, where a melt-drawing ratio of up to 125 changed the crystalline morphology from deformed spherulites to row-nucleated lamellar structure with the lateral size of the lamellar structure ranging between 20 and 40 nm [23]. This crystalline morphology transformation lead to significant improvement of tensile strength and modulus.

In this study, we blended PBS with PaPrHe in an attempt to improve the impact strength of PBS. As high toughness is critical for applications such as electronics and automotive components, enhancing the toughness of PBS is of critical industrial importance to expand the current scope of applications. PBS/PaPrHe binary blends were formed using melt-extrusion and were further processed into both films and injection-molded components. The effects of blend composition on the morphology, thermal and mechanical (tensile, impact strength) properties were analyzed. Further, the blended films were uniaxially stretched and characterized for its tensile strength and change in crystallinity and orientation of molecular chains.

Materials and Methods

Materials

Paramylon was purchased from the Euglena Co. (Tokyo, Japan). Trifluoroacetic anhydride, propionic acid, hexanoic acid, chloroform, methanol, and acetone were purchased from Wako Pure Chemicals (Tokyo, Japan). PBS (M_w:

133,200, M_w/M_n: 1.8, T_m: 114 °C) was procured from Mitsubishi Chemical Corporation, Japan. PaPrHe (M_w: 180,000, M_w/M_n: 2.0, T_m: 137 °C) was synthesized using the procedure described in [14, 24] (Fig. 1). The total degree of substitution was confirmed using NMR to be 3, with Pr:He in 2:1 ratio. For morphological observation, enzymatic etching using *Humicola insolens* cutinase (HiC) was carried out. HiC with an enzyme activity of 15,000 Lipase Unit/g was purchased from Novozymes sold under the tradename Novozym® 51032.

Sample Preparation

Processing of PBS/PaPrHe Blends

PBS and PaPrHe were blended with varying percentage of PaPrHe (10–90 wt%), in a lab-scale melt-kneader (Toyo Seiki, Japan) at 175 °C, 30 rpm for 10 min. The obtained extrudate was then processed to melt-quenched films using a desktop melt-press (Mini Test Press, Toyo Seiki, Japan) at 175 °C for 1 min at 5 MPa. The melt-pressed film was then immediately quenched in an ice-bath for 1 min. Additionally, the extrudate was also made into injection-molded samples using a HAAKE MiniJet Pro, Thermo Scientific, MA, USA under the following conditions: cylinder temperature: 175 °C, mold temperature: 30 °C, injection pressure: 50 MPa, for 20 s.

Selective Etching

To clearly observe the morphology of the PBS rich blend (10–50 wt% PaPrHe), the blended samples were first subjected to enzymatic etching. Since PaPrHe with DS = 3, is not hydrolysable using cutinase and the hydrolysis of PBS was confirmed in literature, PBS was selectively etched in the samples, enabling easy analysis of the phase distribution [25]. Briefly, 10 × 10 mm films were immersed in 2 mL of aqueous HiC solution with a loading of 100 U/mL. The films were then incubated at 45 °C, for up to a week (depending on the PaPrHe loading) with mild shaking. The films after etching were washed with methanol and dried before using in scanning electron microscopy (SEM) analyses. In the case of PaPrHe rich blends, since the HiC etching of PBS was hindered due to the presence of large quantities of PaPrHe, the PaPrHe part was dissolved using acetone and then observed for its morphology.

Uniaxial Drawing of Blended Films

Blended films with up to 30 wt% PaPrHe were uniaxially stretched at 60 °C (near the T_g of PaPrHe) to a draw ratio (DR) of 5 using a hand-held stretching tool. Initially, melt-quenched blended films with up to 30 wt% PaPrHe were fixed to the hand-held stretching tool and thermally equilibrated at 60 °C in an oven for 1 min. After this, the films were stretched to DR 5 manually, followed by annealing at 90 °C for 3 h under tension. The annealing temperature was decided as ~10 °C above the T_g of PaPrHe to possibly allow crystallization of PaPrHe. The films were then allowed to cool to room temperature and used in further characterizations.

Characterizations

Thermal Analysis

Glass transition temperatures (T_g) of PBS/PaPrHe blends were analyzed using a dynamic mechanical analyzer (DMA-8000, PerkinElmer, USA) in single cantilever mode. The heating rate and the frequency of oscillation were set to 2 °C/min and 1 Hz respectively.

The melt-flow temperatures of the blends were measured using a flow-tester (Shimadzu CFT-500EX, Japan) with a heating rate of 3 °C/min and 50 N load attached to a die of diameter 1 mm. The melt-flow temperature was calculated using the offset-temperature method at offset = 5 mm.

Finally, the thermal degradation behavior was tested using a thermogravimetric analysis (Shimadzu TGA-50,

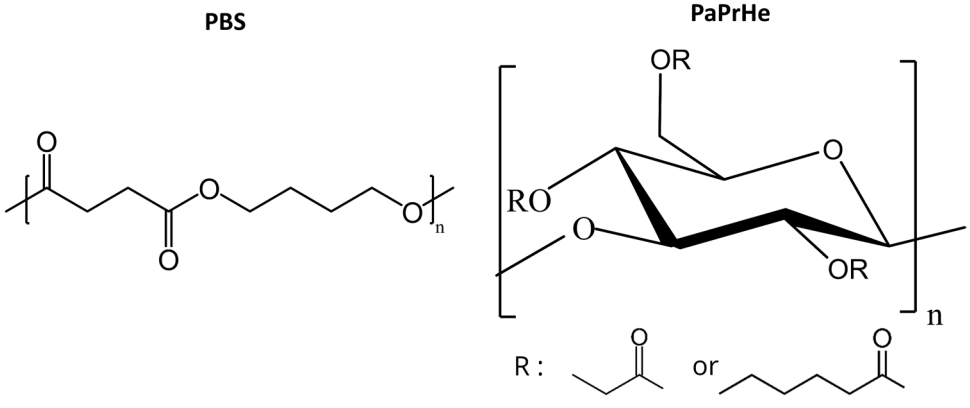

Fig. 1 Chemical structure of PBS and PaPrHe

Japan). About 5–10 mg of test samples were heated from room temperature to 550 °C under nitrogen atmosphere at a heating rate of 10 °C/min. The temperature at 5% degradation, maximum degradation and the residue left were reported.

Surface Morphology

The morphology of the blended samples after selective etching were observed using a desktop SEM (JEOL JCM 7000, Japan) at an accelerating voltage of 15 kV. The samples were sputter coated with gold using a sputter coater (MSP-1S; VACUUM DEVICE) prior to observation.

Mechanical Properties of PBS/PaPrHe Blends

The tensile strength of unstretched blended films were performed as per the ASTM D638 standards in a universal tensile testing machine (Shimadzu EZ-LX, Japan) using a 100 N load cell and strain rate of 50 mm/min. The test samples were cut to shape using a dumbbell cutter (SDL-1000, Dumbbell Co., Ltd., Japan).

The Charpy impact strength was measured according to the ISO 179-1 standards using notched samples. Injection molded samples of dimensions 80 × 10 × 4 mm were notched in the center using a notching tool (A-4 Toyo Seiki, Japan) and were tested in an impact tester (Toyo Seiki, Japan). The striking hammer was fixed with a load of 10 J.

Analysis of Stretch-Annealed Films

The tensile strength of the stretch-annealed films were measured using the same equipment (Shimadzu EZ-LX, Japan), except that the samples were not dumbbell shaped but rather a rectangular strip of 30 × 5 mm.

To evaluate the effect of uniaxial stretching on the crystal structure of the films, Wide-angle X-ray diffraction (WAXD) analysis of the stretch-annealed and control films were carried out. The analysis was done in a Rigaku NANOPIX, Japan ($\lambda = 0.154$ nm) WAXD machine, in the 2θ range of 0°–45°. The camera distance was calibrated using silicon (111) plane as the reference material.

Results and Discussion

Thermal Properties

Thermal properties of polymeric blends, especially the T_g is a good indicator of the compatibility and miscibility of the component polymers as they are strongly related to the interactions between the amorphous regions [26, 27]. The T_g of PBS/PaPrHe blended films after melt quenching is shown in Fig. 2a. Neat PBS showed a T_g of −23 °C, whereas PaPrHe had a higher T_g at 77 °C. In the case of blends, there were two separate T_g observed at the respective temperatures of the PBS and PaPrHe indicating immiscibility in the bulk state [28–32]. When the concentration of PaPrHe was between 10 and 30 wt%, T_g corresponding to PBS did not change much, whereas the PaPrHe T_g shifted to a lower temperature by about 9–13 °C (Table 1). However, on further addition of PaPrHe (from 70 wt%), there was a substantial drop in the T_g of both PBS (by about 11–16 °C) and the PaPrHe part (by 21–23 °C). These results indicate that, at 10–30 wt% PBS concentration, the interaction between these two polymers takes place preferentially in the amorphous region lowering the overall T_g. In addition, the presence of higher quantity of PaPrHe could have probably hindered the crystallization of PBS from the melt, reducing the crystallinity and thereby a decrease in the T_g. This behavior has also been reported previously in PLA/PBS blends at 20 wt% PBS loading [26].

The thermal degradation behavior of PBS/PaPrHe blends was analyzed using thermogravimetric analysis. The TGA and DTG curves are shown in Fig. 2b, c. The temperature at 5% weight loss ($T_{5\%}$) and the temperature of maximum degradation (T_{max}) is given in Table 1. From the results, it could be seen that both PBS and PaPrHe have a high 5% thermal degradation temperature (above 300 °C), with PBS having slightly higher $T_{5\%}$ value. However, after blending, all the samples had a higher $T_{5\%}$ compared to neat PBS and PaPrHe. This behavior could be potentially attributed to the autocatalytic reaction of the evolved by-products during the degradation of either components that can delay the onset of degradation of the blends [33, 34]. On the other hand, T_{max} was seen to be dominated by the higher loading component. This is in accordance with the literature, where partially miscible polymer blends are seen to retain the T_{max} of the individual polymers, probably due to the lack of strong chemical interaction [35].

In terms of melt-processing temperature, the effects of blending were analyzed using a melt-flow tester. The stroke vs. temperature characteristics of PBS/PaPrHe is given in Fig. 2d. The temperature at which the melt flow starts is designated as the reference temperature. Melt-flow temperature (T_{flow}) at offset = 5 mm, mentioned in Table 1 is considered the processing temperature which is defined as the temperature at which the molten polymer can be extruded 5 mm through a die of dia 1 mm, from the reference temperature. T_{flow} of PBS and PaPrHe is 121 °C and 139 °C respectively. With increasing PaPrHe loading, the flow temperature moved closer to that of PaPrHe in the blend, indicating a strong dependence on the PaPrHe concentration (Table 1). In 90 wt% PaPrHe and neat PaPrHe case, the flow is divided into two-steps, the first step at around 60 °C and 80 °C respectively indicating the minor flow of

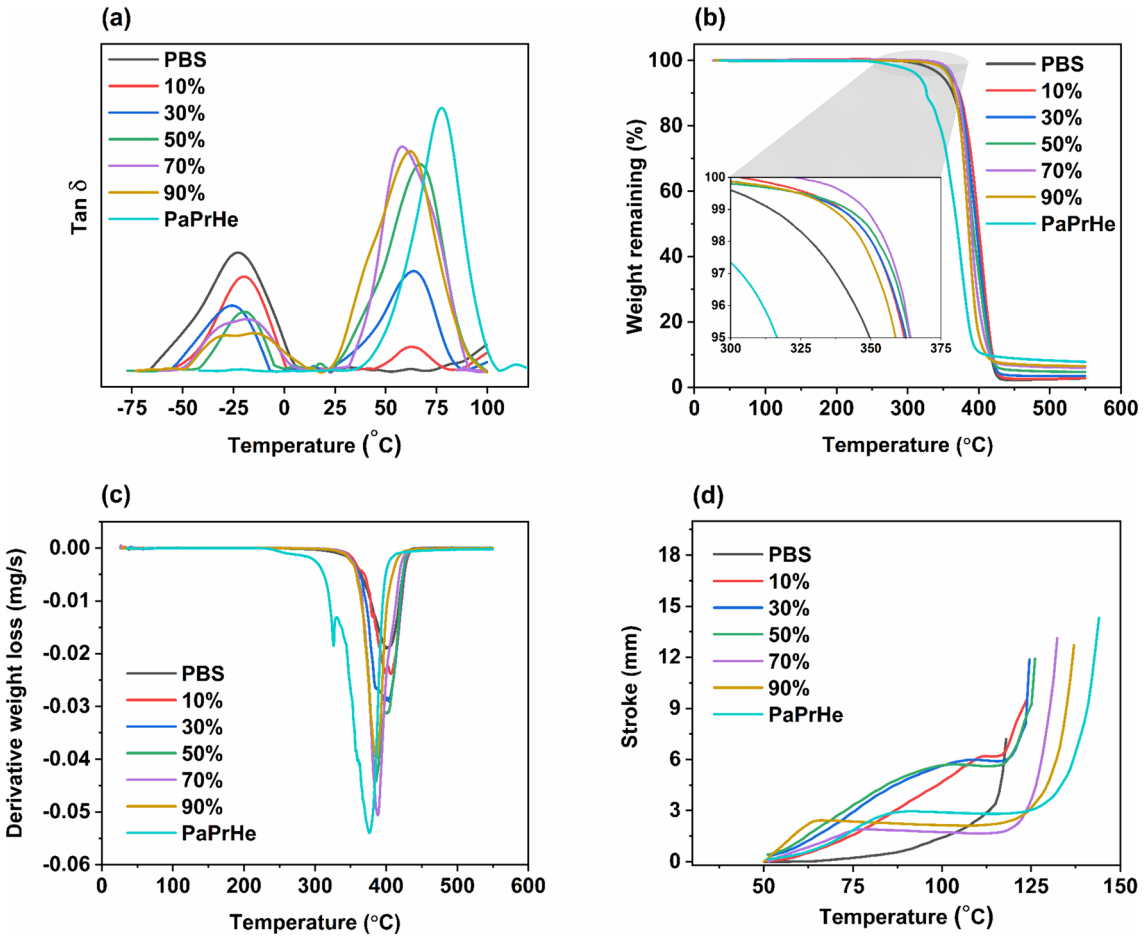

Fig. 2 Thermal properties of PBS/PaPrHe blends **a** Tan δ vs. temperature **b** thermogravimetric analysis **c** derivative thermogravimetric analysis **d** melt-flow curve. The percentage in the figure legends indicate the PaPrHe wt %

Table 1 Summary of thermal properties of PBS/PaPrHe blend

PaPrHe loading (wt%)	DMA		TGA			Melt flow tester
	[a]T_g (°C)	[b]T_g (°C)	[c]$T_{5\%}$ (°C)	[d]T_{max} (°C)	Residual weight (%)	[e]T_{flow} (°C)
0	−23	–	350	400	2.7	121
10	−21	64	362	406	2.8	124
30	−24	64	363	404	3.5	124
50	−20	68	364	385	4.8	126
70	−39	54	364	388	6.0	129
90	−34, −11	56	359	385	6.5	133
100	–	77	316	376	7.8	139

[a]T_g of PBS (Peak top in the Tan δ curve)

[b]T_g of PaPrHe (Peak top in the Tan δ curve)

[c]Temperature of 5% degradation (from TGA curve)

[d]Temperature of maximum weight loss (from DTG curve)

[e]Melt flow temperature defined as the temperature at stroke = 5 mm

the molecular chains under load, or in other words the glass transition. These temperatures also align with the values from DMA (Fig. 2d). In the second step, at around 125 °C, the major melt-flow starts for both the samples. However,

such two-step transition was not seen in other samples, probably due to domination of PBS in melt-flow characteristics, which has a glass transition temperature significantly lower than the test window. Overall, the flow temperature in all the samples are lower than the $T_{5\%}$, suggesting that they can be processed into various form without undergoing thermal degradation.

Surface Morphology

The SEM images of the PBS/PaPrHe blend after selective etching are shown in Fig. 3. In the 10 wt% PaPrHe blend, several uniformly dispersed etched-PBS islands with diameter about 6–8 µm are seen (Fig. 3a). Larger islands of diameter 13–20 µm are also seen, probably formed after the etching of nearby-smaller islands. On further magnification of these PBS-islands, we can observe pores of diameter up to 2 µm (median dia 0.9 µm) (Fig. 3b, c). Increasing the PaPrHe loading to 30 wt%, the larger PBS islands become less-distinct, however the PBS-pores are seen more uniformly dispersed across the surface (Fig. 3d). The median dia in the 30 wt% PaPrHe case was 2 µm (Fig. 3e, f). The broadening of the pore size distribution is attributed to the coalescence of PBS particles during the kneading process [36]. Up until this point, the PaPrHe loading is only about 10–30 wt% in the blend, which should ideally translate to the majority of the bulk surface (representative of PBS) be etched/porous, however that is not the case. This suggests that a major part of the unetched surface is comprised of partially miscible PBS/PaPrHe phase as also hinted by the DMA results. Presence of non-hydrolysable PaPrHe in the partially miscible phase might have restricted the etching of PBS.

When the PaPrHe loading was increased to 50 wt%, the phase morphology transitioned to a co-continuous system with the median diameter of the PBS-phase (represented by the etched holes) being 13 µm (Fig. 3g). Furthermore, spherical beads of median dia 2.3 µm can also be seen scattered across the surface beneath the etched PBS (Fig. 3g inset). The 70 wt% and 90 wt% PaPrHe ratios were selectively etched using acetone in this study. The morphology remained co-continuous in both these cases, with the etched holes representing PaPrHe, visible in the SEM images (Fig. 3h, i). Increasing of PaPrHe ratio did not result in any clear phase transition. However, since the effects of acetone

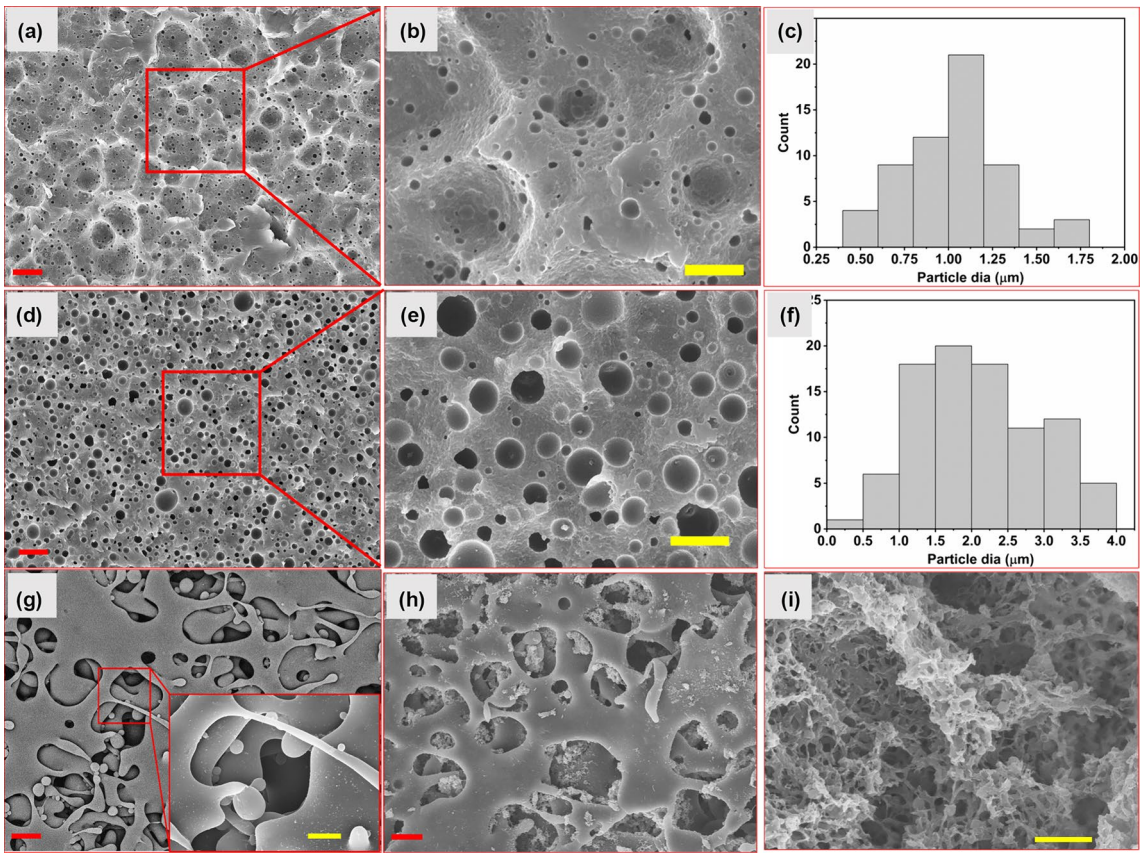

Fig. 3 SEM images of PBS/PaPrHe blends after enzymatic etching using HiC or acetone treatment. **a**, **b** 10 wt% PaPrHe **c** particle size distribution of 10 wt% PaPrHe **d**, **e** 30 wt% PaPrHe **f** particle size distribution of 30 wt% PaPrHe **g** 50 wt% PaPrHe **h** 70 wt% PaPrHe **i** 90 wt% PaPrHe. The red scale bar represents 10 µm and the yellow scale bar represents 5 µm

on the swelling and dilation of partially miscible phase are not clear, quantitative discussion on the phase sizes is avoided. Further analysis on the micro-structure needs to be carried out to quantify the domain sizes.

Crude estimation of the amount of PaPrHe in the partially miscible phase was determined for the blended samples (*see supplementary information for more details*). It was found that, in the lower loading ratios of PaPrHe (10 wt%, 30 wt%), majority of the loaded PaPrHe (up to 25.3 wt%) could be credited to be involved in the formation of partially miscible PBS/PaPrHe phase. At further loading (50–90 wt%), this value remained more or less the same at around 24–26 wt%. These results indicate that, the saturation of partially miscibility has been achieved at around 30 wt% PaPrHe loading, beyond which there is not much thermodynamic miscibility between these two polymers. In the blended samples with up to 30 wt% PaPrHe, since the majority of the blended PaPrHe was involved in the partially miscible phase, we could see almost no neat PaPrHe beads in the SEM images. On the other hand, at higher loading of PaPrHe (>50 wt%), since a saturation in partial miscibility was achieved, the remaining amount of PaPrHe not included in the partially miscible phase could have formed the spherical beads as observed in Fig. 3g. The presence of partially miscible micro-phase with no clear interfacial gaps can enhance the secondary interactions between PBS and PaPrHe and give rise to unique physical properties [37, 38]. In particular, co-continuous domain with micron-sized beads in the 50 wt% PaPrHe blend is expected to have a significant impact on the mechanical properties of the blend.

Mechanical Properties

The tensile properties of PBS/PaPrHe are presented in Fig. 4. All the blended films showed a characteristic low elastic, large plastic deformation with significant strain hardening behavior before fracture (Fig. 4a). It has been widely reported that for polymers with large elongation, tensile stress-resistance is attributed to the orientation of the molecular chains and the extension of chain conformation. As a result, neat PBS showed an yield strength of 21.8 MPa and the highest strength at break (73.8 MPa), along with its typical stress-oscillation behavior as a result of secondary-recrystallisation [39, 40]. Compared to PBS, PaPrHe is less flexible, as the mobility of molecular chains is limited due to its higher T_g. Neat PaPrHe had a yield strength of 18.9 MPa, elongation at break: 87% and strength at break of 27.8 MPa. Incorporating PaPrHe in the PBS matrix resulted in loss of elongation and strength at break. At 10 wt% PaPrHe loading, there was a ~30% reduction in both elongation and strength compared to neat PBS. The higher standard deviation in the 10% PaPrHe loading could be potentially attributed to the stretching of PaPrHe microbeads. From the particle size distribution in Fig. 3c, a considerable number of particles in the 10% PaPrHe blend were that with a diameter <1 µm. These smaller diameter particles may undergo stretching together with the PBS domain during the tensile test, resulting in increased elongation in certain samples. Conversely, when the particles do not undergo stretching, it leads to stress concentration and premature failure. The larger error could be from the heterogeneous distribution of the smaller diameter particles within the blend. When PBS was blended with 30 wt% PaPrHe, the elongation at break and strength at break decreased by about 50% (Fig. 4b). However, the Young's modulus and yield strength seem to have had no significant change up to 50 wt% PaPrHe loading (Fig. 4b). Further increase in PaPrHe wt% (70 and 90 wt%), the tensile properties were similar to neat PaPrHe films, with slightly lower strength at break.

The impact strength is one of the most versatile tools to analyze the toughness of a material. In this study, Charpy notched impact tests were carried out, and the results are given in Fig. 5. PBS had the lowest impact strength (6.6 kJ/m^2) out of all the samples. In the case of 10 wt% PaPrHe

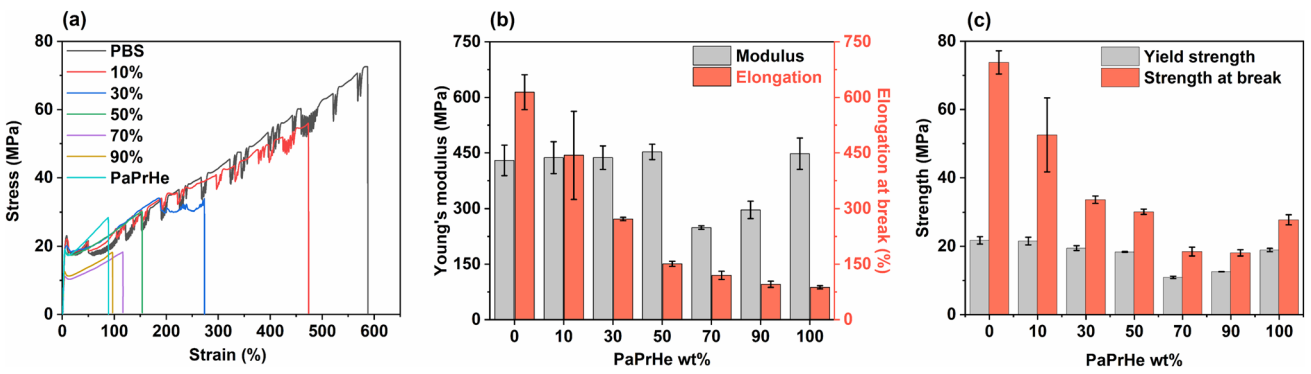

Fig. 4 Tensile properties of PBS/PaPrHe blends **a** Stress–strain curves. The percentage in the figure legends indicate the PaPrHe wt %. **b** Young's modulus and elongation at break. **c** Yield strength and strength at break

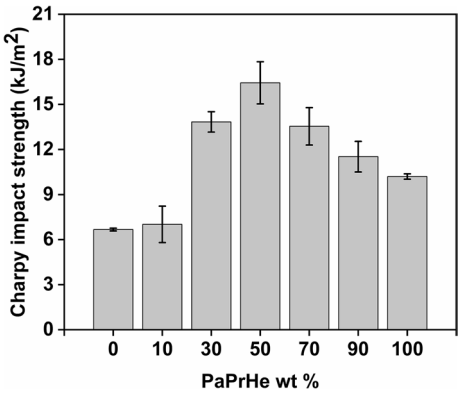

Fig. 5 Notched Charpy impact strength of PBS/PaPrHe blend

blend, there was no substantial improvement in the toughness of PBS. However, with increasing PaPrHe wt%, the toughness of PBS/PaPrHe blends improved significantly. For example, at 30 wt% PaPrHe, the toughness of the blends increased by over 100% (13.8 kJ/m^2) and with further incorporation of PaPrHe, (50 wt%), the toughness was enhanced by over 140% (16.4 kJ/m^2), the highest in this study. On increasing the PaPrHe wt% to 70–90%, the toughness value was higher than neat PBS, but at this point, it is unfair to compare the toughness with PBS as the bulk majority is of PaPrHe. Nevertheless, the impact strength at these ratio were higher than neat PaPrHe, which could be potentially attributed to the co-continuous morphology of the blend. With respect to impact fracture, all the impact strength samples fractured completely, unlike hinge type fracture exhibited in other PaPrHe based blends [15].

In terms of the mechanical properties of PBS/PaPrHe blend, the inclusion of PaPrHe had a positive impact on the toughness of the blends, however had a generally weakening effect on the tensile strength and elongation at break. This behavior can be explained by the morphology of the blend and its subsequent effect on the fracture mechanism in either case. Typically, tensile properties, particularly the elongation at break of polymeric blend is highly dependent on the interfacial adhesion between the phases, in this study, PBS, PaPrHe and the partially miscible PBS/PaPrHe phase. Introduction of PaPrHe in PBS blends decreased the elongation at break significantly. As PaPrHe is the more rigid component, a strong interfacial interaction could have therefore restricted the molecular mobility of PBS leading to stress-concentration and subsequent loss in elongation at even a low loading of 10 wt% PaPrHe.

In sudden impact loading, the deformation is mainly controlled by the occurrence of crazing mechanism [41, 42]. Under crazing, when a sudden force acts on a bulk polymer, micro voids or microcracks are formed ahead of the main crack propagation tip which delays the onset of bulk failure, thereby increasing the impact energy absorbed. Out of the several factors that affects crazing, the size of particles and stress-concentration are two major parameters. In the case of PBS/PaPrHe blend, these two factors worked in favor for the successful improvement in the toughness of the blend. The presence of PaPrHe particles increases the stress-concentration in the blend due to the difference in the particle geometry between PBS and PaPrHe [43]. From the SEM images, it can be seen that the median particle dia of 10 wt% PaPrHe blend was about 0.9 µm, as opposed to the 2.3 µm in the 30 wt% PaPrHe blend. When the dispersed phase is <1 µm, stress-concentration formed during the impact loading is low due to which the crazes are unable to propagate further. But, if the dispersed particle is ≥1 µm, the stress-concentration is sufficient enough to sustain the craze-propagation. Under such a case, the crack propagation would be dominated by a large number of small crazes that delays the fracture [42].

Overall, in terms of mechanical properties of the PBS/PaPrHe blend, the domain size formed had a positive impact on the toughness but had a negative effect on the tensile performance. The highest toughness value (16.4 kJ/m^2) was obtained in 50 wt% PaPrHe ratio having a co-continuous morphology with micron-sized beads dispersed homogeneously. On the other hand, tensile properties gradually decreased with increasing PaPrHe% with the best performance in 10 wt% PaPrHe blends (Strength and elongation at break: 52 MPa and 443% respectively).

Properties of Uniaxially Stretched Films

One of the key applications of bio-based PBS is in packaging owing to its reduced carbon footprint, higher thermal stability and processability. Typically, in packaging, films are often stretched and oriented to improve the properties such as strength, durability, printability and to reduce the material usage (thereby lower cost). In an ideal situation, blending with PaPrHe should not hinder the applicability of PBS in these applications. So, in this work, PBS/PaPrHe blends were subjected to uniaxial drawing to a stretched-to draw ratio (DR) of 5 and checked for its tensile properties. Films with more than 50 wt% PaPrHe were not able to be stretched, so were not included in the analysis.

The tensile strength of DR 5 films is compared to their unstretched counterparts in Fig. 6. It must be read with caution and considered only as a reference since the standards used in both the testing are different. But clearly the tensile strength at break has improved by over 230–380% in the stretched films compared to the unstretched neat films. The strength at break slightly dropped in the blended samples compared to neat PBS, however, it is noteworthy that the 10 wt% and 30 wt% PaPrHe blend had tensile strength (200 MPa and 165 MPa) about 80% and 70% of the neat PBS stretched film respectively. For comparison, the strength at break of typical stretched bio-based films for packaging

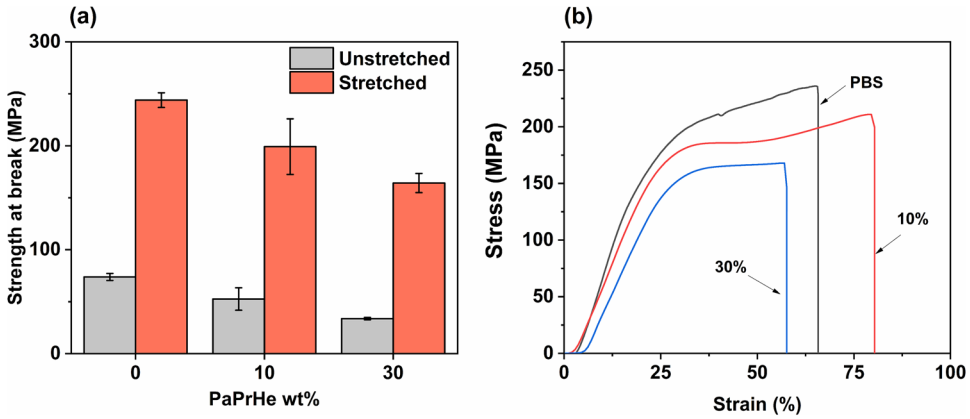

Fig. 6 **a** Strength at break of unstretched and DR 5 stretch-annealed films. **b** Stress–Strain curve of PBS/PaPrHe DR 5 stretch-annealed films. The percentage indicates the PaPrHe wt %

applications, such as PLLA or poly(butylene succinate-*co*-adipate) ranged between 120 and 180 MPa in the literature [15, 44]. Hence, PBS/PaPrHe blends can be potentially used in the stretched-film industry without any strength issues.

The results from X-ray diffraction studies of the stretch annealed films are given in Fig. 7. Typical diffraction peaks at 2θ: 19.7° and 22.8° ascribed to the (020) and (110) plane are visible [45]. In the 2D WAXD images of neat-unstretched annealed films, ring-like patterns indicative of no-orientation of the crystals could be seen with the overall crystallinity ranging between 28% and 35%. With increasing PaPrHe ratio, ring corresponding to the PaPrHe in the low Bragg's angle region also becomes evident. On stretching the films to DR 5 and annealing, both neat PBS films and blended films showed highly oriented diffraction patterns associated with PBS and PaPrHe. The degree of orientation calculated from the Azimuthal's profile of (110) was 95% in all three samples. The higher strength at break in the stretched films could be a direct result of the higher degree of orientation, since there was no significant change in the percentage crystallinity. This leads to the possibility that the probable drop in tensile strength in the blended samples could be attributed to (a) micro-voids or micro-cracks developed during stretching or (b) insufficient crystallization. Basically, the annealing of the stretched films was carried at 90 °C, (10–15 °C higher than the T_g of PaPrHe), which is closer to the melting point of PBS. During stretching, smaller imperfect crystals are developed by the transformation of the mobile amorphous fraction into rigid amorphous fraction. These smaller crystals could be partially melted and converted back to liquid-like mobile amorphous fraction at temperatures close to the T_m, leading to no significant improvement in the crystallinity. In addition, the crystallization rate is drastically retarded at higher crystallization temperature for PBS [28]. Hence, further optimizing the drawing and annealing conditions could improve the tensile performance of PBS/PaPrHe stretched films, with even little or potentially no drop in tensile strength.

Conclusions

Binary blends from PBS and PaPrHe were prepared and characterized for its miscibility, morphology, and physical properties. The PBS/PaPrHe blend system was partially miscible, however, the morphology was considerably different with varying PaPrHe content. At lower concentrations (10–30 wt% PaPrHe), sea-island morphology with sub-micron to micron order domain sizes were seen which transformed into a co-continuous mesh like morphology in the ratios with >50

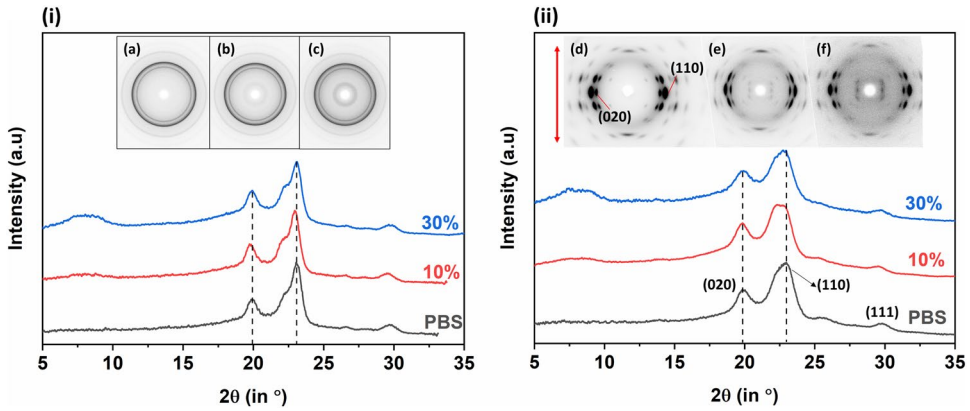

Fig. 7 **i** One dimensional diffraction curves of unstretched-annealed PBS/PaPrHe blended films. (Inset) *a–c* 2D WAXD images of PBS, 10 wt% and 30 w% PaPrHe respectively. **ii** One dimensional diffraction curves of DR5-annealed PBS/PaPrHe blended films. (Inset) *d–f* Corresponding 2D WAXD images of PBS, 10 wt% and 30 wt% PaPrHe respectively. Red arrow indicates the stretching axis

wt% PaPrHe. Crude estimation indicated that up to 25 wt% of PaPrHe was included in the partially miscible phase which improved the interfacial interaction between PBS and PaPrHe. In terms of mechanical properties, with increasing PaPrHe wt% the impact strength of PBS increased from 6.6 kJ/m^2 to up to 16.4 kJ/m^2, almost a 150% increase. Tensile strength on the other hand decreased by almost 30%, even at a low loading of 10 wt% PaPrHe due to the rigid nature of PaPrHe compared to PBS. Further addition of PaPrHe only worsened the tensile properties. This loss could be partially countered by uniaxially stretching the blended films with up to 30 wt% PaPrHe to a draw ratio of 5, where high tensile strengths of up to ~200 MPa comparable to PLA stretched films could be achieved. The enhancement in tensile strength was attributed to the increased degree of orientation of the crystals in the blend. Overall, the blending of PBS with PaPrHe is a simple yet effective and scalable way to improve the toughness of PBS. The effects of morphology on other properties such as tear strength and gas barrier properties of the blends needs to be analyzed for a much clearer image of industrial applications. However, bio-based PBS/PaPrHe blends possess properties that could be useful in electronics and automotive components, in addition to sustainable packaging and mulching applications.

Supplementary Information The online version contains supplementary material available at https://doi.org/10.1007/s10924-024-03274-w.

Acknowledgements This work was supported by the New Energy and Industrial Technology Development Organization (Grant Number: JPNP20008), Japan. A part of this work was funded by the Grants-in-Aid for Scientific Research (A) (No. 19H00908) from the Japan Society for the Promotion of Science (JSPS), Japan to Tadahisa Iwata. Manikandan Ilangovan thanks the Ministry of Education, Culture, Sports, Science and Technology—Japan for funding through the MEXT Scholarship. A part of the WAXD analyses were carried out in SPring-8, synchrotron radiation facility. The beamtime was granted through the proposal numbers: 2022B1405 and 2023A7204.

Author Contributions MI: Investigation, Data Curation, Visualization, Writing—original draft. TK: Methodology, Supervision, Writing—Review and Editing. TI: Conceptualization, Writing—review and editing, Supervision, Funding acquisition.

Funding Open Access funding provided by The University of Tokyo.

Data Availability Data are available upon reasonable request from the corresponding author.

Declarations

Conflict of interest The authors declare no competing financial interest.

References

1. Rosenboom J-G, Langer R, Traverso G (2022) Bioplastics for a circular economy. Nat Rev Mater 7:117–137. https://doi.org/10.1038/s41578-021-00407-8
2. Iwata T (2015) Biodegradable and bio-based polymers: future prospects of eco-friendly plastics. Angew Chem Int Ed 54:3210–3215. https://doi.org/10.1002/anie.201410770
3. Platnieks O, Gaidukovs S, Kumar Thakur V et al (2021) Bio-based poly(butylene succinate): recent progress, challenges and future opportunities. Eur Polym J 161:110855. https://doi.org/10.1016/j.eurpolymj.2021.110855
4. Barletta M, Aversa C, Ayyoob M et al (2022) Poly(butylene succinate) (PBS): materials, processing, and industrial applications. Prog Polym Sci 132:101579. https://doi.org/10.1016/j.progpolymsci.2022.101579
5. Tachibana Y, Masuda T, Funabashi M, Kunioka M (2010) Chemical synthesis of fully biomass-based poly(butylene succinate) from inedible-biomass-based furfural and evaluation of its biomass carbon ratio. Biomacromolecules 11:2760–2765. https://doi.org/10.1021/bm100820y
6. Wang H, Gan Z, Schultz JM, Yan S (2008) A morphological study of poly(butylene succinate)/poly(butylene adipate) blends with different blend ratios and crystallization processes. Polymer 49:2342–2353. https://doi.org/10.1016/j.polymer.2008.02.050
7. Lindström A, Hakkarainen M (2007) Designed chain architecture for enhanced migration resistance and property preservation in poly(vinyl chloride)/polyester blends. Biomacromolecules 8:1187–1194. https://doi.org/10.1021/bm070001k
8. Goffin A-L, Habibi Y, Raquez J-M, Dubois P (2012) Polyester-grafted cellulose nanowhiskers: a new approach for tuning the microstructure of immiscible polyester blends. ACS Appl Mater Interfaces 4:3364–3371. https://doi.org/10.1021/am3008196
9. Gan H, Enomoto Y, Kabe T et al (2017) Synthesis, properties and molecular conformation of paramylon ester derivatives. Polym Degrad Stab 145:142–149. https://doi.org/10.1016/j.polymdegradstab.2017.05.011
10. Feuzing F, Mbakidi JP, Marchal L et al (2022) A review of paramylon processing routes from microalga biomass to non-derivatized and chemically modified products. Carbohydr Polym 288:119181. https://doi.org/10.1016/j.carbpol.2022.119181
11. Piiparinen J, Barth D, Eriksen NT et al (2018) Microalgal CO_2 capture at extreme pH values. Algal Res 32:321–328. https://doi.org/10.1016/j.algal.2018.04.021
12. Rubiyatno MT, Mori K, Toyama T (2021) Paramylon production by *Euglena gracilis* via mixotrophic cultivation using sewage effluent and waste organic compounds. Bioresour Technol Rep 15:100735. https://doi.org/10.1016/j.biteb.2021.100735
13. Shibakami M, Sohma M (2017) Synthesis and thermal properties of paramylon mixed esters and optical, mechanical, and crystal properties of their hot-pressed films. Carbohydr Polym 155:416–424. https://doi.org/10.1016/j.carbpol.2016.08.093
14. Shibakami M, Tsubouchi G, Sohma M, Hayashi M (2015) One-pot synthesis of thermoplastic mixed paramylon esters using trifluoroacetic anhydride. Carbohydr Polym 119:1–7. https://doi.org/10.1016/j.carbpol.2014.11.036
15. Ilangovan M, Gan H, Kabe T, Iwata T (2022) Preparation and properties of binary green blends from poly(butylene

succinate-co-adipate) and β-(1,3)-d-glucan ester derivative. Polymer 259:125332. https://doi.org/10.1016/j.polymer.2022.125332
16. Zhao T, Yu J, Zhang X et al (2023) Thermal, crystallization, and mechanical properties of polylactic acid (PLA)/poly(butylene succinate) (PBS) blends. Polym Bull 81:1–24. https://doi.org/10.1007/s00289-023-04848-9
17. Zhao T, Yu J, Pan H et al (2023) Super-tough polylactic acid (PLA)/poly(butylene succinate) (PBS) materials prepared through reactive blending with epoxy-functionalized PMMA-GMA copolymer. Int J Biol Macromol 251:126150. https://doi.org/10.1016/J.IJBIOMAC.2023.126150
18. Shi K, Liu Y, Hu X et al (2018) Preparation, characterization, and biodegradation of poly(butylene succinate)/cellulose triacetate blends. Int J Biol Macromol 114:373–380. https://doi.org/10.1016/j.ijbiomac.2018.03.151
19. Tatsushima T, Ogata N, Nakane K, Ogihara T (2005) Structure and physical properties of cellulose acetate butyrate/poly(butylene succinate) blend. J Appl Polym Sci 96:400–406. https://doi.org/10.1002/app.21451
20. Tachibana Y, Giang NTT, Ninomiya F et al (2010) Cellulose acetate butyrate as multifunctional additive for poly(butylene succinate) by melt blending: mechanical properties, biomass carbon ratio, and control of biodegradability. Polym Degrad Stab 95:1406–1413. https://doi.org/10.1016/j.polymdegradstab.2010.01.006
21. Ilangovan M, Gan H, Kabe T, Iwata T (2023) Bio-based polymer blend with tunable properties developed from paramylon hexanoate and poly(butylene succinate). Polymer 270:125791. https://doi.org/10.1016/j.polymer.2023.125791
22. Vega-Baudrit J, Pereira R, Nakayama K et al (2004) Structure and properties of biodegradable polymers: rolling effect in poly(butylene succinate) sheets. Polym Polym Compos 12:63–73. https://doi.org/10.1177/096739110401200106
23. Xie J, Yin L, Wu Y et al (2021) The effect of the melt-drawing ratio on the microstructure and mechanical properties of poly(butylene succinate) cast films with row-nucleated lamellar structure. Polym Test 104:107394. https://doi.org/10.1016/J.POLYMERTESTING.2021.107394
24. Ilangovan M, Kabe T, Iwata T (2023) Investigating the structure-property relationships of paramylon ester/PBAT blends for sustainable packaging. ACS Appl Polym Mater 5:9255–9262. https://doi.org/10.1021/acsapm.3c01759
25. Huang Q, Kimura S, Iwata T (2023) Thermal embedding of *Humicola insolens* cutinase: a strategy for improving polyester biodegradation in seawater. Biomacromolecules. https://doi.org/10.1021/acs.biomac.3c00835
26. Im D, Gavande V, Lee H et al (2021) Compatibility and hydrolytic behaviors of polylactide isomer/poly(butylene succinate) mixtures by the Langmuir technique. Polym Degrad Stab 186:109517. https://doi.org/10.1016/j.polymdegradstab.2021.109517
27. Supthanyakul R, Kaabbuathong N, Chirachanchai S (2016) Random poly(butylene succinate-co-lactic acid) as a multi-functional additive for miscibility, toughness, and clarity of PLA/PBS blends. Polymer 105:1–9. https://doi.org/10.1016/j.polymer.2016.10.006
28. Zhu W, Wang X, Chen X, Xu K (2009) Miscibility, crystallization, and mechanical properties of poly(3-hydroxybutyrate-co-4-hydroxybutyrate)/poly(butylene succinate) blends. J Appl Polym Sci 114:3923–3931. https://doi.org/10.1002/app.30965
29. Jeepery IF, Sudesh K, Abe H (2021) Miscibility and enzymatic degradability of poly(3-hydroxybutyrate-co-3-hydroxyhexanoate)-based polyester blends by PHB depolymerase and lipase. Polym Degrad Stab 192:109692. https://doi.org/10.1016/j.polymdegradstab.2021.109692
30. Jeepery IF, Goto T, Sudesh K, Abe H (2023) Biodegradable block copolymer as compatibilizer and blend component of poly(3-hydroxybutyrate-co-3-hydroxyhexanoate)-based polyester blends. Eur Polym J 196:112314. https://doi.org/10.1016/J.EURPOLYMJ.2023.112314
31. Chen F, Zhang J (2010) Effects of plasticization and shear stress on phase structure development and properties of soy protein blends. ACS Appl Mater Interfaces 2:3324–3332. https://doi.org/10.1021/am100751c
32. Hernández MC, Laredo E, Bello A et al (2002) From miscible to immiscible polycarbonate/poly(ε-caprolactone) blends. Macromolecules 35:7301–7313. https://doi.org/10.1021/ma0204655
33. Thaumaturgo C, Monteiro EC (1997) Thermal stability and miscibility in PVC/EVA blends. J Therm Anal 49:247–254. https://doi.org/10.1007/BF01987445
34. Salazar Avalos A, Hakkarainen M, Odelius K (2017) Superiorly plasticized PVC/PBSA blends through crotonic and acrylic acid functionalization of PVC. Polymers 9:84. https://doi.org/10.3390/polym9030084
35. Lizymol PP, Thomas S (1993) Thermal behaviour of polymer blends: a comparison of the thermal properties of miscible and immiscible systems. Polym Degrad Stab 41:59–64. https://doi.org/10.1016/0141-3910(93)90061-M
36. Pesaranhajiabbas E, Pal AK, Rodriguez-Uribe A et al (2022) Biodegradable polymer blends: studies on performance control through droplet to co-continuous morphology. ACS Appl Polym Mater 4:5546–5556. https://doi.org/10.1021/acsapm.2c00603
37. Xu H, Zhou J, Odelius K et al (2021) Nanostructured phase morphology of a biobased copolymer for tough and UV-resistant polylactide. ACS Appl Polym Mater 3:1973–1982. https://doi.org/10.1021/acsapm.1c00057
38. Suchao-in K, Koombhongse P, Chirachanchai S (2014) Starch grafted poly(butylene succinate) via conjugating reaction and its role on enhancing the compatibility. Carbohydr Polym 102:95–102. https://doi.org/10.1016/j.carbpol.2013.11.001
39. Wan C, Heeley EL, Zhou Y et al (2018) Stress-oscillation behaviour of semi-crystalline polymers: the case of poly(butylene succinate). Soft Matter 14:9175–9184. https://doi.org/10.1039/C8SM01889H
40. Huang Q, Kimura S, Iwata T (2021) Development of self-degradable aliphatic polyesters by embedding lipases via melt extrusion. Polym Degrad Stab 190:109647. https://doi.org/10.1016/j.polymdegradstab.2021.109647
41. Ethier JG, Drummy LF, Vaia RA, Hall LM (2019) Uniaxial deformation and crazing in glassy polymer-grafted nanoparticle ultrathin films. ACS Nano 13:12816–12829. https://doi.org/10.1021/acsnano.9b05001
42. Jang BZ, Uhlmann DR, Vander SJB (1985) The rubber particle size dependence of crazing in polypropylene. Polym Eng Sci 25:643–651. https://doi.org/10.1002/pen.760251011
43. Sallal HA, Abdul-Hamead AA, Othman FM (2020) Effect of nano powder (Al_2O_3-CaO) addition on the mechanical properties of the polymer blend matrix composite. Def Technol 16:425–431. https://doi.org/10.1016/j.dt.2019.07.013
44. Park JW, Doi Y, Iwata T (2004) Uniaxial drawing and mechanical properties of poly[(R)-3-hydroxybutyrate]/poly(L-lactic acid) blends. Biomacromolecules 5:1557–1566. https://doi.org/10.1021/bm0499051
45. Gan Z, Abe H, Kurokawa H, Doi Y (2001) Solid-state microstructures, thermal properties, and crystallization of biodegradable poly(butylene succinate) (PBS) and its copolyesters. Biomacromolecules 2:605–613. https://doi.org/10.1021/bm015535e